Magnetic Resonance in Medicine 41:72–79 (1999)

Performance of a High-Temperature Superconducting Probe for In Vivo Microscopy at 2.0 T

Jason R. Miller,[1]* Sarah E. Hurlston,[2] Q. Y. Ma,[1] Dean W. Face,[3] Dennis J. Kountz,[3] James R. MacFall,[2] Laurence W. Hedlund,[2] and G. Allan Johnson[2]

The use of a high-temperature superconducting probe for in vivo magnetic resonance microscopy at 2 T is described. To evaluate the performance of the probe, a series of SNR comparisons are carried out. The SNR increased by a factor of 3.7 compared with an equivalent copper coil. Quantitative measures of the SNR gain are in good agreement with theoretical predictions. A number of issues that are unique to the application of HTS coils are examined, including the difficulty in obtaining homogenous excitation without degrading the SNR of the probe. The use of the HTS probe in transmit-receive mode is simple to implement but results in nonuniform excitation. The effect of using the probe in this mode of operation on the T_1 and T_2^* contrast is investigated. Methods for improving homogeneity are explored, such as employing a transmit volume coil. It is found that the cost of using an external transmit coil is an increased probe noise temperature and a reduced SNR by ~30%. Other important aspects of the probe are considered, including the effect of temperature on probe stability. Three-dimensional in vivo imaging sets are acquired to assess the stability of the probe for long scans. High-resolution images of the rat brain demonstrate the utility of the probe for microscopy applications. Magn Reson Med 41:72–79, 1999. © **1999 Wiley-Liss, Inc.**

Key words: in vivo microscopy; high-temperature superconductors (HTS); radio-frequency (RF) coils; superconducting resonators

INTRODUCTION

Studies in magnetic resonance microscopy (MRM) typically require high spatial resolution that places extraordinary demands on the signal-to-noise ratio (SNR). This is especially true if isotropic 3D volume imaging is required to avoid partial volume effects. To increase the SNR, there are a number of factors that can be optimized. For sufficiently small samples, the losses from the RF coil are large in comparison with the sample losses (1), which means that RF coils optimized to reduce coil loss can be used to greatly improve the SNR. Surface coils made of high-temperature superconducting (HTS) material have the potential for drastically reduced coil loss and increased sensitivity. Several studies have demonstrated their use and have reported substantial SNR gains (1,2). However, use of these probes for microscopy has been limited to in vitro applications. The use of HTS probes for in vivo applications results in unique concerns and challenges that we address in this paper.

One issue that is unique to the application of HTS probes is the difficulty in achieving homogeneous excitation without substantially degrading the SNR of the probe. The inherent RF inhomogeneity of surface coils produces a spatially nonuniform excitation. Surface coils are routinely used with a separate decoupled transmit volume coil to achieve a more uniform RF excitation. The challenge with HTS probes is to decouple the coils while preserving the SNR of the probe. One technique for decoupling the coils is orienting the B_1 fields (the alternating magnetic field produced by the RF coil) orthogonal to each other (3). However, decoupling is difficult to achieve in practice (4) since surface coils produce a B_1 that varies its orientation depending on position. Other schemes for decoupling have been shown to degrade the SNR by introducing active or passive elements into the electrical circuit (3,5). Such noise contributions become even more intolerable in the context of the low HTS coil noise. There is also the possibility of using the surface coil without compensating for the spatially nonuniform excitation. The use of a single surface coil avoids the problem of decoupling and has the added advantage of simplicity, only one coil occupying the bore space. But using the HTS coil in transmit-receive mode results in nonuniform T_1 weighting throughout the field of view (FOV), since the combination of excitation angle and TR determines the amount of T_1 weighting. To overcome the problems with the nonuniform RF field that result from the single-coil HTS design, an HTS Helmholtz pair was recently demonstrated for microscopy at 9.4 T (6). However, the current probe construction is not suitable for in vivo imaging studies and still suffers from RF inhomogeneity.

Another issue of importance is the stability of the HTS probe during imaging experiments. This is a problem because of the precise tuning and matching that is required for high Q coils. Microscopy scans routinely use high-resolution 3D acquisitions that require long scan times. The probe must be stable for the duration of the experiment.

In this paper, we report on the performance of an HTS probe for in vivo microscopy studies, and we address some of the issues involved with the use of HTS probes. We begin by evaluating the SNR performance of the HTS probe by comparing phantom images obtained with an HTS coil with that of a conventional copper surface coil of similar geometry. These data are then compared with estimates of the SNR based on the measured coil Q value, noise

[1]Department of Electrical Engineering, Columbia University, New York, New York.

[2]Center for In Vivo Microscopy, Duke University Medical Center, Durham, North Carolina.

[3]Dupont, Wilmington, Delaware.

Grant sponsor: NIH-NCRR; Grant number: P4105959; Grant sponsor: NSF Career Awards.

This work was performed in part at Duke University, Center for In Vivo Microscopy.

*Correspondence to: Jason R. Miller, Ph.D., Motorola, 3501 Ed Bluestein Boulevard, Austin TX, 78731 MD:K20.

Received 10 November 1997; revised 25 May 1998; accepted 28 May 1998.

temperature, and coil inductance. Next we look at alternatives for achieving a suitable excitation profile, including the use of an external volume coil. The effect of the transmit volume coil on the SNR is analyzed by measuring the SNR in receive-only mode with the transmit volume coil and in transmit-receive mode. To explore the limitations of imaging in receive-only mode, images of a rat brain are acquired at different transmit powers. Other important aspects of the probe, such as the effect of temperature on the probe stability, are described. Images are presented to demonstrate the probe stability and the SNR advantage. Imaging of rats is specifically targeted because of the high resolution that is required to adequately render the features of the rat brain and because of its frequent use in studies of biological importance.

THEORY

HTS coils can provide a higher SNR by lowering the noise contribution of the coil and increasing the coil sensitivity. These characteristics are indicative of a coil having a low noise temperature and a high Q value. Significant SNR gains can be achieved from HTS coils at low operating frequencies and small sample sizes based on the scaling laws (1). Under these conditions, the sample resistance (electrical resistance appearing in the coil circuit attributable to sample electrical losses) is found to be less than the coil resistance. The SNR improvement that can be achieved by employing HTS coils, as compared with a conventional room-temperature copper coil, depends upon the sample resistance, coil resistance, coil inductance, and noise temperature of the HTS and copper coil. Measurement of the loaded and unloaded Q provides a means of determining the coil and sample resistance. The coil and sample resistance can be calculated using the following formulas: $R_C = \omega L/Q_U$ and $R_s = \omega L(1/Q_L - 1/Q_U)$, where L is the coil inductance, ω is the resonant frequency of the coil, Q_L and Q_U are the loaded and unloaded Q, and R_C and R_S are the coil and sample resistance. The noise voltages generated by the coil, sample, and preamplifier represent three different noise sources that need to be accounted for in SNR calculations. These three noise sources can be simply added, and an effective noise temperature T_{eff} can be defined as (7)

$$T_{eff} = T_n + \frac{R_S T_S + R_C T_C}{R_S + R_C} \quad [1]$$

where T_n and T_C are the noise temperatures of the preamplifier and coil, respectively, and T_S is the physical temperature of the sample. The SNR for each coil can be expressed as

$$\text{SNR} \propto \sqrt{\frac{Q_L}{T_{eff} L}} \quad [2]$$

The predicted SNR improvement can be calculated by dividing the SNR values obtained from Eq. [2] for the HTS coil and copper coil. Note that this computation of SNR assumes that the B fields are identical for the two coils.

MATERIALS AND METHODS

Coil Design and Measurement of Q

The HTS coil was made from $Tl_2Ba_2CaCu_2O_8$ (TBCCO) thin film on 2-inch diameter single crystal $LaAlO_3$ substrate (8). The critical temperature (T_c) of the film is about 104 K. The coil design consists of a single turn inductor with interdigital capacitors (9) between the inner and outer portions of the turn (10). A numerical, mathematical model that included the detailed coil parameters was used for calculating the resonant frequency of the coil. Fine tuning of the coil was accomplished by laser trimming the interdigital fingers, thus reducing the capacitance and increasing the resonant frequency. The coil was specifically designed for the geometric region of interest (ROI) to optimize the SNR. In this case, the coil size was made large enough to include the rat brain within the sensitive volume of the coil. The outer and inner diameters of the coil are 2.45 and 1.8 cm, respectively. The inductor linewidths are 274 μm, and the interdigital fingers are on average 234 μm wide and spaced 144 μm apart. To facilitate comparison with the HTS coil, an equivalent copper coil was constructed. The 2.4-cm diameter copper coil consisted of a single turn of 3-mm diameter copper wire with a low loss trimmer capacitor in parallel with a fixed capacitance (Dielectric Labs, Cazenovia, NY). The copper coil was placed as close to the sample as possible for the imaging experiments to maximize the SNR. Offsetting the copper surface coil from the sample can improve the SNR when the decrease in noise due to loading outweighs the loss in signal strength associated with withdrawing the coil (11). For microscopy studies, the sample resistance is usually small compared with the copper coil resistance, which means that as the coil is withdrawn, the total resistance (coil + sample) stays about the same but the signal decreases rapidly, lowering the SNR.

In addition to the copper surface coil, the performance of the HTS coil was compared with an Alderman-Grant volume coil. The resonator was 3 cm in diameter and 4 cm long. It consisted of two 3-cm loops of copper tubing (0.317-cm diameter) connected by a 1 × 4 cm sheet of Cuflon capacitor material. This coil was specifically designed for microscopy of the rat brain studies, and was optimized to maximize both Q and the filling factor.

A modified Alderman-Grant resonator was constructed to be used as an external excitation coil. The coil windings were made from copper foil and a low loss trimmer capacitor was used to form the resonant circuit. The uniformity of the RF transmit field was verified using a Wavetek bridge in conjunction with a sweep generator and a small pickup loop. The receive coils were decoupled from the transmit coil by orthogonal positioning before imaging.

The resonant frequency and Q of the coils were determined using a 4194A network analyzer (Hewlett Packard, Palo Alto, CA), using the S11 mode. Because the Q of the HTS coil depends on incident power, an internal attenuator was used to reduce the input power. Measurements were made at a temperature of 30 K unless otherwise specified. Note that the term ''unloaded Q'' refers to the Q when the coil is not loaded by the sample or the coupling

circuit. The unloaded Q can be found by doubling the loaded Q when the coil is matched. However, the actual Q seen by the spins will be half this value when the HTS coil is matched to the coupling circuit and preamplifier. Inductance measurements on the copper coil were performed using a 4274A LCR meter (Hewlett Packard, Palo Alto, CA). The noise temperature of the HTS coil was measured using the hot/cold resistor method (12). The method uses the imaging spectrometer to measure noise voltages produced by 50 Ω terminations at 300 and 77 K. Then the HTS probe, matched to 50 Ω, was measured, and the noise temperature was calculated.

Experimental Setup

The HTS coils were positioned in a custom-designed liquid helium flow cryostat, described elsewhere (13), adapted for use in a 2.0 T microscopy system. The cryostat was supported in a Plexiglas cylinder that was shielded by a 36-μm thick copper shield (All Foils, Inc., Brooklyn Heights, OH). The Plexiglas tube is easily moved in the bore, which helps in positioning the coil at gradient center. With the position of the cryostat fixed, the animal position can be varied until the ROI is located. All experiments were performed with the static B_o field parallel to the plane of the HTS coil. This is done because magnetic fields normal to the superconducting film plane increase the loss due to the anisotropy of the superconductor (14). Thermal shielding limits the minimal coil-sample separation to about 4 mm for the HTS coil. A Lakeshore 330 temperature controller maintained the temperature of the coil throughout the experiment at 30 ± 0.01 K using a proportional, integral, derivative (PID) control algorithm. The temperature of the coil was monitored by a platinum thermometer.

When the cryostat was operating, fine tuning of the resonant frequency for a given sample was accomplished by adjusting the position of a small copper tab that intercepts some of the flux of the HTS coil and decreases its effective inductance. The effect of the copper tab is an elevation of the resonant frequency so that the coil must be made to resonate slightly below the Larmor frequency to ensure that the coil can be properly tuned. The copper tab and coupling loop were thermally anchored to the copper cold block to reduce the thermal noise of the HTS circuit. Low loss matching of the HTS coil was accomplished by using an inductively coupled pickup loop. By adjusting the proximity of the loop to the coil, the coefficient of coupling can be varied so that the source impedance can be transformed to 50 (1). Before imaging, the coils were tuned to the resonant frequency of 85.53 MHz and matched to 50 Ω. A GE preamplifier originally designed for use at 1.5 T was modified for use at 2.0 T.

Animal Preparation and Support

Female rats (n = 5), about 155 g body weight (Fisher 344, Charles River Laboratories, Wilmington, MA), were prepared in accordance with procedures approved by the Duke University Institutional Animal Care and Use Committee. The five animals were used in five different imaging experiments. They were anesthetized with an intraperitoneal injection of pentobarbital sodium (38 mg/kg, Abbott Labs, North Chicago, IL) and given atropine sulfate (35 mg/kg, Vedco, Inc., St. Joseph, MO), and then perorally intubated (16-gauge intravenous cannula, Sherwood Medical, Tullamore, Ireland). An intraperitoneal catheter (22-gauge, Quik-Cath, Baxter, Deerfield, IL) was established to periodically administer supplemental doses of anesthesia. Electrocardiogram (ECG) electrodes (pediatric) were taped to the foot pads, and a thermistor was inserted into the rectum. Physiological signals were processed (Coulbourn Instruments, Allentown, PA) and displayed continuously on a Macintosh computer (Apple Computer, Inc., Cupertino, CA) with an A/D board and a LabVIEW (National Instruments, Austin, TX) program (15). Animal body temperature during imaging was controlled using warmed air circulating through the magnet bore, a feedback control loop from the rectal thermistor, and a process control loop in the physiologic monitor application (16). Animals were maintained in this way for up to several hours. Body temperature from study to study ranged from 34 to 37°C. In some studies, lower than desirable body temperatures occurred because the HTS probe assembly restricted the circulation of warm air past the animal. This was later remedied by making an air passage in the bore to allow the warm air to pass unrestricted. For imaging, the animal was supported by a Plexiglas platform that allowed positioning of the head within a few millimeters of the probe and parallel with it.

Imaging Experiments

All imaging was performed on a 30-cm horizontal bore magnet dedicated to MRM. The systems employ shielded gradient coils delivering a peak gradient of 18 Gauss/cm. The system is controlled by a GE Signa console modified to operate as a broadband imaging system up to 85 MHz. We chose a gradient-recalled acquisition in the steady-state (GRASS) sequence for two reasons. First, the use of a spin-echo sequence with B_1 inhomogeneity reduces the signal intensity in regions where the excitation and refocusing pulse angles deviate from the ideal values of 90 and 180°, respectively, producing image artifacts. Second, the use of a single RF pulse with GRASS results in a signal away from the surface coil that falls off at a rate $B_1\sin(\Theta)$, where Θ is the position-dependent flip angle. However, in the spin-echo case, the signal falls off as $B_1\sin^3(\Theta)$. Thus, the signal will be attenuated much more quickly, and the effective FOV will be substantially reduced. Imaging parameters were chosen that best suited each comparison being made. Details about the imaging parameters can be found in the accompanying Figure legends.

SNR Comparisons

SNR measurements were carried out with homogenous phantoms made to simulate the loading of a rat head. The phantom consisted of a 10-cc syringe filled with saline solution having a similar physiologic conductivity of 0.5 S/m. Images of the phantom were obtained using the HTS coil, copper coil, and the HTS coil with the transmit volume coil. The SNR of the images was evaluated using MATLAB (The Math Works, Natick, MA).

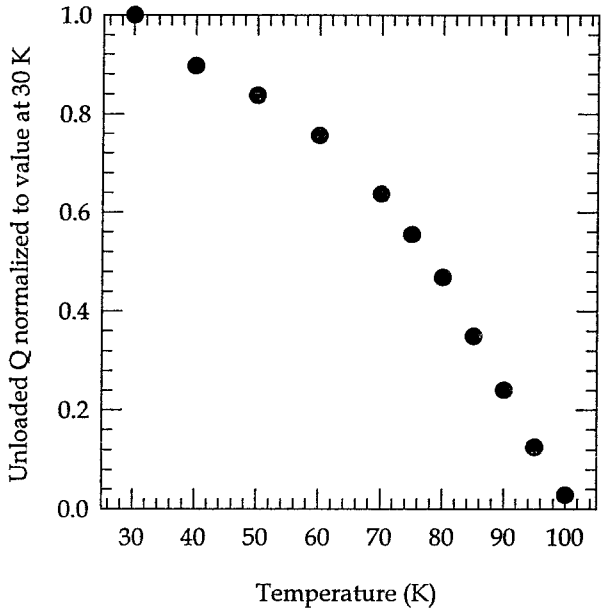

FIG. 1. Plot of the unloaded *Q* versus temperature at zero field. *Q* values are normalized to 24,000, which was the *Q* value measured at 30 K.

Image reconstruction and visualization were performed on a Silicon Graphics computer using locally written software. To evaluate the SNR gain of the HTS probe, intensity images were generated that mapped the SNR across the image. The SNR was calculated using a signal region of 4×4 pixels and a noise region of 50×50 pixels to ensure accuracy within 10% (17). The SNR was calculated for the entire image, and the maximal SNR values for each image were compared.

RESULTS AND DISCUSSION

Q Measurements and Frequency Stability

The unloaded *Q* of the HTS coil was found to be about 24,000 at 30 K. The effect of temperature on the unloaded *Q* at zero field is shown in Fig. 1. The *Q* values are normalized to the *Q* value measured at 30 K. This behavior can be understood by the simple two-fluid theory of a superconductor. There is qualitative agreement between these data and data obtained for YBCO coils (2). In the field, the unloaded *Q* decreased to about 18,000 as a result of the introduction of vortex flux structures. The addition of a copper shield slightly increased the *Q*. This is because the shield reduces the loss due to radiation. It has been pointed out previously that the *Q* is limited by radiation resistance (18). Tuning of the coil provides an additional loss mechanism. The magnetic field of the HTS coil induces eddy currents in the copper tab, which causes power to be dissipated by the resonator. Tuning the coil to the frequency required for imaging (85.53 MHz) lowered the *Q* of the HTS coil in field to about 5500. The saline phantom loaded the *Q* in field to about 4400. The *Q* values measured are summarized in Table 1. The effect of tuning on the loaded *Q* is shown in Fig. 2 at zero field (at 30 K). Here, the term ''loaded *Q*'' refers to the load introduced by the copper tab. *Q* values are normalized to the maximal loaded *Q* value (~9000) that was measured at 85.16 MHz, corresponding to the natural resonant frequency of the coil. Figure 2 stresses the importance of minimizing the tuning that is required for the HTS coil to achieve high *Q* values. Although tuning is required to adjust for sample loading, the resonant frequency of the coil should be as close as possible to the frequency for imaging to optimize *Q*. This demands careful processing of the coil and good predictive models of the coil resonant frequency. To obtain accurate readings of the unloaded *Q*, the input power of the network analyzer was attenuated iteratively until the *Q* no longer increased. This was found to occur at about −40 dBm. The power dependence of one of the HTS coils in field is shown in Fig. 3. The *Q* values are normalized to the *Q* value measured at −40 dBm.

Table 1
Summary of Measured *Q* Values

Conditions	HTS coil	Copper coil
Unloaded matched *Q* (0 T)[a]	12,000	150
Unloaded matched *Q* (2 T)	9000	150
Tuned	5500	150
Loaded *Q* (phantom)	4400	140

[a]The actual internal *Q* of the coil is twice the unloaded matched *Q* value.

Q measurements were made on the copper surface coil and Alderman-Grant resonator. The unloaded *Q* of the copper coil was 150 and reduced to about 140 when loaded by the saline phantom. The Alderman-Grant resonator had an unloaded *Q* of about 500.

An important consideration for stable operation of the probe is the temperature-dependent frequency shift of the HTS coil. The natural resonant frequency versus tempera-

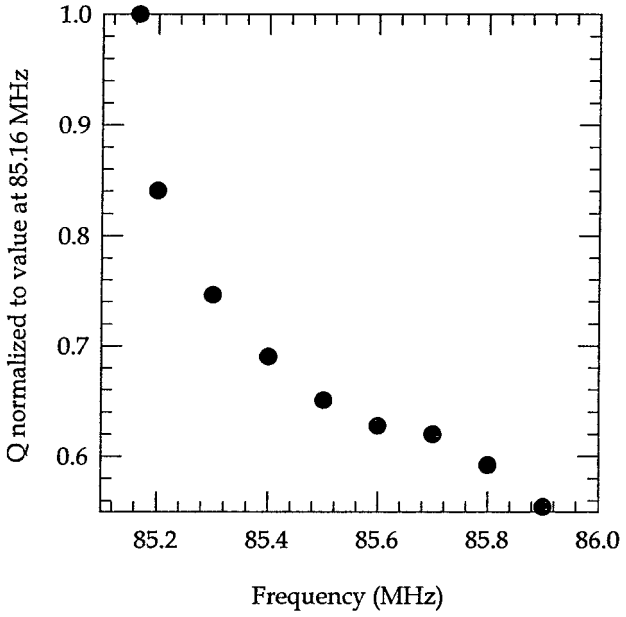

FIG. 2. Plot of the loaded *Q* as a function of coil tuning at zero field. The untuned or natural resonance frequency of the coil was 85.16 MHz at 30 K. Imaging required that the coil be tuned to 85.53 MHz.

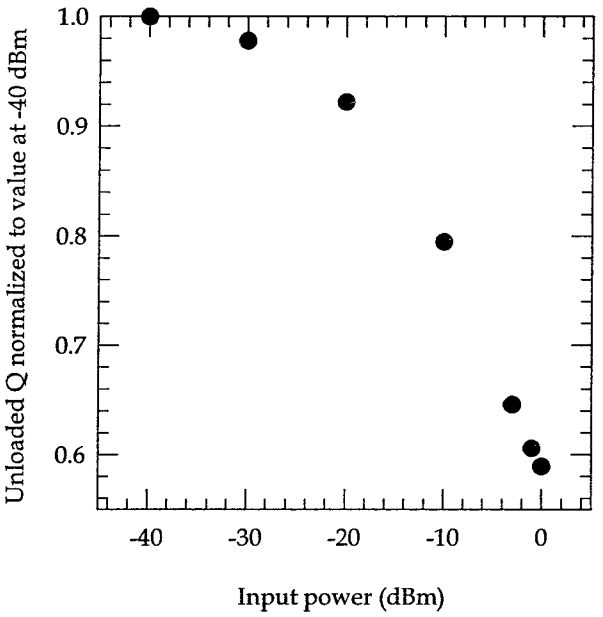

FIG. 3. Plot of the unloaded Q versus input power at zero field. Q values only slightly improve for input powers <-30 dBm. The resonant frequency of the coil is also a function of input power.

ture of one of the HTS coils is shown in Fig. 4. At low temperatures (below about 70 K), the frequency is observed to decrease linearly with temperature. This can be simply related to the thermal expansion of the substrate. At higher temperatures, the frequency shift can be attributed to the change of the electromagnetic field distribution as a consequence of the change in the penetration depth (19). This is manifested as a sharp increase of frequency with decreasing temperature. Figure 4 shows that the coil must be operated at temperatures well below T_c for stability. At temperatures slightly below T_c, small temperature fluctuations result in large changes of the resonant frequency, but at lower temperatures, the resonant frequency is less sensitive to temperature fluctuations. The other benefits of low-temperature operation are decreased Johnson noise and higher Q values. In addition to operating at temperatures well below T_c to reduce the sensitivity of the coil to temperature fluctuations, the high Q of the HTS coil makes accurate temperature control essential to stay within the narrow 3 dB bandwidth. We found that with the appropriate PID settings on the temperature controller, the coil temperature could be stabilized to ± 0.01 K after an initial cool-down period.

SNR Measurements Compared with Theory

To predict the SNR advantage of the HTS coil, the Q, noise temperature, and inductance of the HTS coil and copper coil were determined. The copper coil inductance was measured to be about 55 nH using the LCR meter described above. The inductance of the HTS coil was estimated to be about 137 nH by Wheeler's formula modified for the case of a printed circuit spiral coil (20). The noise temperature of the HTS coil in receive-only mode was found to be high, about 179 K. Since the physical temperature of the coil is about 30 K, there are additional noise sources that are coupled to the coil. These noise sources include the RF shield and the metal portions of the cryostat, such as the radiation shield. The addition of the transmit volume coil dramatically increased the noise temperature of the HTS coil to about 580 K. The noise temperature of the preamplifier was about 73 K, which is equivalent to a noise figure of about 1.25 dB or a 25% SNR degradation. Inserting these values and the values for the unloaded and loaded Q reported above into Eqs. [1] and [2], the SNR advantage of the HTS coil over the copper coil was predicted to be greater by a factor of 4.0, and the SNR of the HTS coil in transmit-receive mode was predicted to be greater by a factor of 2.7.

SNR measurements were made on saline-filled phantoms. Figure 5 plots the SNR that was obtained from phantom images as a function of transmit power attenuation using (a) an HTS coil in transmit-receive mode, (b) an HTS coil in receive-only mode with the transmit volume coil, and (c) a copper surface coil. In each series, the transmit attenuation was varied from 20 to 30 dB in steps of 1 dB. For the three coil configurations, maximal SNR was achieved at a transmit attenuation that resulted in a 90° flip angle. In the case of (a) and (c), this means that the surface of the phantom, where the sensitivity of the coil is greatest, has reached a flip angle of 90°. Note that for the volume coil, the sensitivity is fairly uniform, so that the maximal SNR is not localized within the volume. The maximal SNR of the HTS coil in transmit-receive mode was found to be greater by a factor of 3.7 than the copper coil image, whereas the SNR of the HTS coil in receive-only mode was found to be greater by a factor of 2.8 than the copper coil image. Good quantitative agreement is found between the predicted and measured SNR gain. The error bars shown in Fig. 5 include the scan-to-scan image variance and the error in determining the SNR of each image using the MATLAB program. To determine the error bars, 10 images were acquired using identical image parameters and condi-

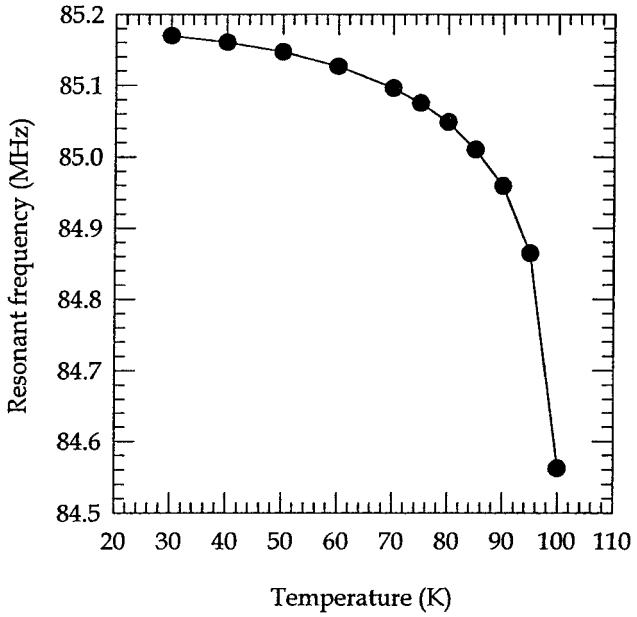

FIG. 4. Plot of the natural resonant frequency versus temperature at zero field.

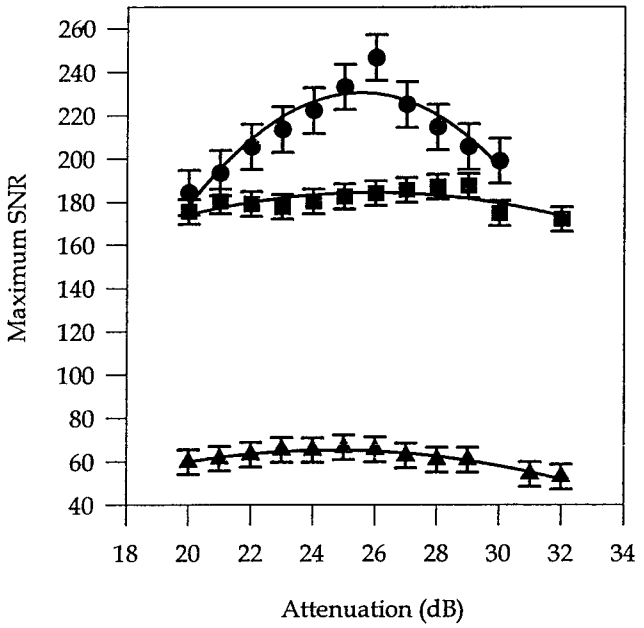

FIG. 5. Plots of maximal SNR versus transmit power attenuation shown for (a) the HTS coil in transmit-receive mode (●), (b) the HTS coil in receive-only mode with the transmit volume coil (■), and (c) the copper surface coil (▲). The error bars were determined from the standard deviation.

tions. The MAT-LAB program then calculated the SNR of the 10 images, and the error bars were determined from the standard deviation of the SNR. This process was repeated for each coil configuration.

The presence of the transmit coil reduced the SNR advantage of the HTS coil by about 24% (from 3.7 to 2.8). The high noise temperature of the HTS coil with the transmit coil indicates that the transmit coil is adding significant Johnson noise to the HTS coil, which reduces the SNR gain. For conventional surface coils, the use of orthogonal transmit coils is a solution to the homogeneity problem, but for HTS coils, with their low noise attributes, the approach will not fully exploit the SNR gains. Active decoupling techniques will not improve the situation because it is the noise added by the presence of the transmit coil that degrades the SNR. Larger diameter transmit coils (not possible here) or specialized decoupling electronics may be possible solutions. Note that the measurement of the SNR change due to the introduction of the volume coil is preferred to the measurement of the change in Q (5). In fact, after the coils were decoupled, no drop in the Q of the HTS coil was observed.

Considering the high probe noise temperature, the improvement in SNR is predominantely from the probe's increased sensitivity. That is, the current induced by the spin system in the pickup coil will produce a voltage that is proportional to Q. It is apparent from Eqs. [1] and [2] that lowering the probe noise temperature will result in higher SNR gains. We can use the measurement data of the Q and inductance to estimate the gains that can be achieved by reducing the noise temperature. For example, a reduction of the coil noise temperature to 20 K, which was achieved by Black *et al.* (2), is predicted to increase the SNR gain by a factor of about 1.5. To significantly decrease the noise temperature of the HTS probe in transmit-receive mode, one can reduce the noise coupled to the HTS circuit by cooling the RF shield. This approach, taken by Black *et al.*, has been shown to substantially increase the SNR (2). If the probe noise temperature were reduced to 20 K, it would make sense to concentrate our efforts on reducing the noise temperature of other aspects of the receiver chain, such as the preamplifier, because the noise temperature of the preamplifier becomes a greater proportion of the total noise temperature of the receiver chain. Cooling the preamplifier in liquid nitrogen (77 K) has resulted in preamplifiers that have noise temperatures of 10 K (1). Lowering the probe noise temperature to 20 K and employing a cooled preamplifier with a noise temperature of 10 K could conceivably increase the SNR gain by a factor of about 1.8. Future work will be focused on reducing the noise temperature of the receiver chain.

In Vivo Imaging Experiments

The initial group of experiments with the transmit volume coil and HTS coil established that the use of the volume coil results in SNR degradation. Based on this fact, we chose to do without the transmit volume coil for the in vivo experiments to fully exploit the SNR gains and to evaluate the performance of the HTS probe in transmit-receive mode. Figure 6 shows axial images of a rat brain obtained

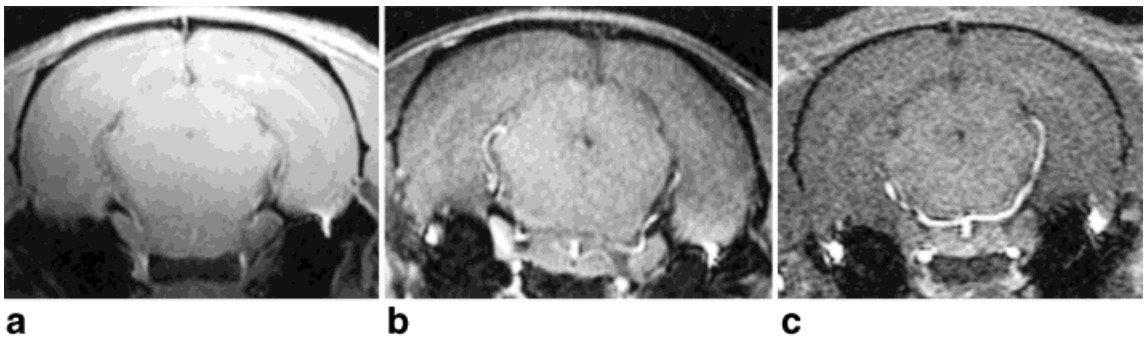

FIG. 6. In vivo axial rat images obtained with (a) the HTS coil in transmit-receive mode, (b) the copper coil, and (c) the Helmholtz-type volume coil. The image acquisition parameters were identical: a 3D GRASS scan, TR 100 ms, TE 4 ms, and NEX 1. The data matrix is $256 \times 192 \times 64$ over an FOV of 3×3 cm. Similar slices were chosen from the 3D data sets.

with an HTS coil (Fig. 6a), a copper surface coil (Fig. 6b), and an Alderman-Grant volume coil (Fig. 6c). As with the phantom experiments, the transmit power attenuation was adjusted to achieve a 90° flip angle at the surface of the head. We attempted to choose similar physiological slices from the 3D data sets to make the comparisons meaningful. The SNR advantage of the HTS coil is apparent as evidenced by the grainier appearance of Figs. 6b and 6c. It is not surprising to see a surface coil outperform a volume coil, but the comparison is intended to provide insight into their relative performance. Although quantitative measure of the SNR gain is less accurate than phantom comparisons, the SNR of Fig. 6a was found to be greater by a factor of 4 than Fig. 6b and greater by a factor of 6 than Fig. 6c. Note that three different rat specimens were used for Figs. 6a–6c although the rats were similarly sized, each weighing about 150 g.

The lack of B_1 homogeneity leads to nonuniform T_1 weighting throughout the FOV. The images of Fig. 7 show the effect of changing the transmit power on the T_1 contrast of the image using the HTS coil in transmit-receive mode. The rat image shown in Fig. 7a was tipped $<90°$ across the entire image, which produced an essentially proton density-weighted image. By increasing the transmit power, the image shown in Fig. 7b has obtained a flip angle of 90° at the surface. Note that although Fig. 7b has little contrast, it measures the highest SNR. The image shown in Fig. 7c was tipped slightly $>90°$ at the surface. This power setting was found to optimize the T_1 contrast. Therefore, the conditions for maximal SNR may not optimize the contrast-to-noise ratio (CNR) over a desired portion of the imaging volume. The transmit power in Fig. 7c was 4 dB greater than in Fig. 7b, which, from Fig. 5, reduced the SNR by about 20%. Further increasing the power reduced the contrast. Despite the B_1 inhomogeneity, Fig. 7c shows that good T_1 contrast can be achieved across the brain.

We next put the probe to the task of acquiring 3D image sets with the T_1 weighting adjusted as in Fig. 7c and with a T_2^*-weighted sequence. Several TE values were explored. A TE of 25 ms was chosen to give some T_2^* weighting without too great a signal loss. Figure 8 shows representative images from the two 3D data sets from about the same position in the brain. Figure 8a is representative of a T_1-weighted image, and Fig. 8b is representative of a T_2-weighted image. The in-plane resolution of both images is <50 μm. High SNR is evidenced by the lack of graininess in the images. Figure 8a shows excellent separation between the cortex, corpus callosum, and hippocampus. Figure 8b shows radiating vascular detail in the cortex arising from blood oxygen level dependent contrast (BOLD) (21). Note, in particular, the detail seen in Fig. 8c, a 2× magnification of Fig. 8b. In this particular image, the 50-μm in-plane resolution is certainly helpful in resolving the vascular detail. Yet the sensitivity provided by the HTS coil is sufficient to provide the differential contrast necessary to highlight these small vessels.

The 64 slices per scan required a total acquisition time of about 80 min. After each scan, the resonant frequency of the HTS coil was found to have drifted by about 5 kHz. The drift is well within ½ Q of the resonant frequency. In fact, calculation shows that the coil current is maintained to 94% of the resonant current with the coil 5 kHz off resonance (22). The stability offered by this probe is essential for practical in vivo microscopy, which routinely uses high-resolution 3D acquisitions that require long scan times. Further efforts to improve the probe stability will be focused on damping mechanical vibrations induced by the gradients and on implementing a more robust tuning scheme with perhaps less Q degradation.

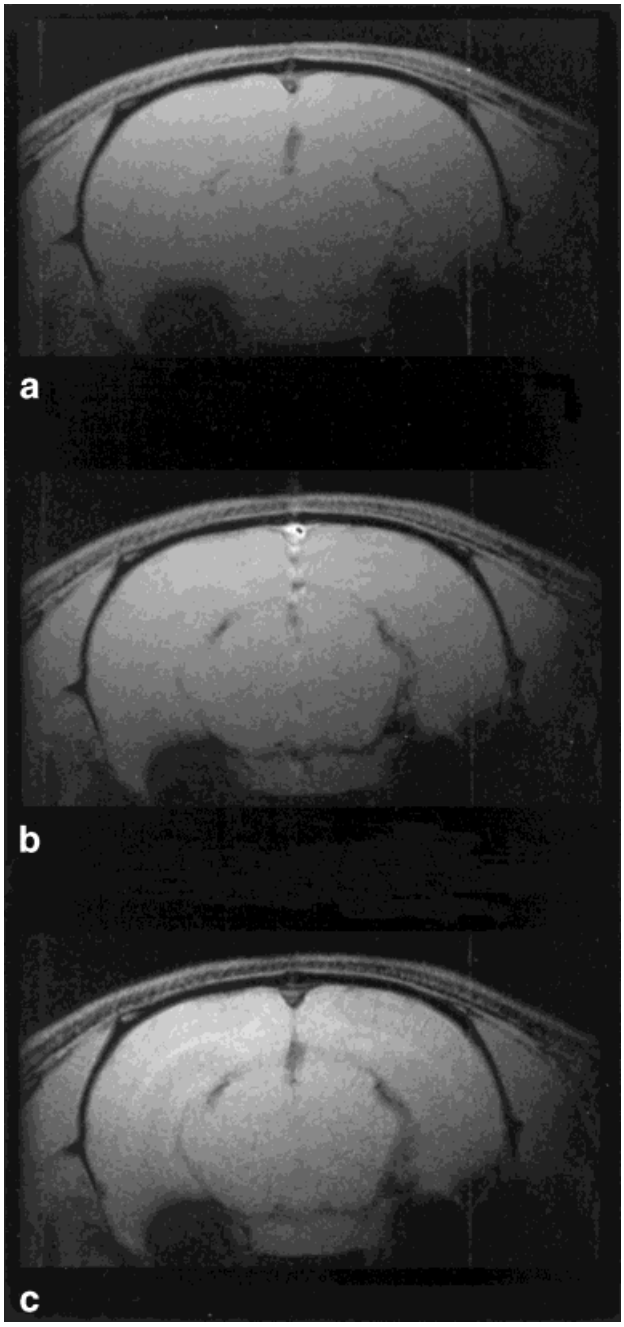

FIG. 7. In vivo axial rat images obtained with the HTS coil in transmit-receive mode. The transmit power attenuation was adjusted such that the flip angle at the surface was (a) $<90°$, (b) 90°, and (c) $>90°$. The image acquisition parameters were a 2D GRASS scan, TR 200 ms, TE 9 ms, and NEX 8. The data matrix is 512 × 512 over an FOV of 2 × 2 cm.

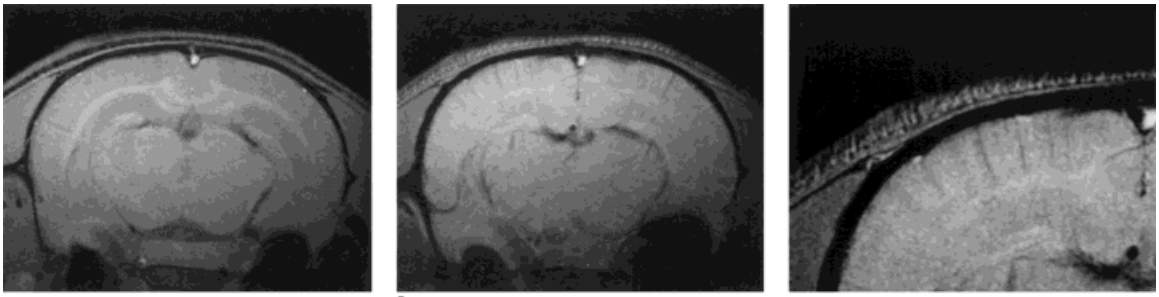

FIG. 8. In vivo axial rat images obtained with the HTS coil in transmit-receive mode with (a) TE 9 ms and (b) TE 25 ms. A 2× magnification of (b) is shown in (c). The image acquisition parameters were a 3D GRASS scan, TR 150 ms, and NEX 1. The data matrix is 512 × 512 × 64 over an FOV of 2.5 × 2.5 cm, yielding resolution of 49 × 49 × 500 μm.

CONCLUSIONS

The SNR improvements achieved with the current HTS probe represent an improvement of more than 3× over that of a conventional copper surface coil. The use of a single coil does have some problems arising from B_1 inhomogeneity, which limits the utility of some pulse sequences. Traditional approaches limiting B_1 inhomogeneity during transmit by use of an external volume coil degrade the SNR of the HTS coil by ~30%. Operation of the coil in transmit-receive mode is, therefore, the configuration of choice. In this configuration, the system is clearly applicable in a wide range of in vivo microscopy studies.

The cryostat and animal support elements have been addressed to permit stable, robust operation over sufficient acquisition periods to make the probe extremely useful for MRM. T_1- and T_2^*-weighted images have been demonstrated with acceptable contrast variations over the restricted 20–30 mm field of view. The example images with in-plane resolution of 50 μm allow superb definition of microvasculature in the brain. No doubt, other applications will be readily demonstrated in the spine and bodies of smaller rodents. Careful analysis of the noise sources suggests that there are still improvements to be made by reducing the noise temperature of the HTS coil. The work here clearly demonstrates that HTS coils can deliver the significant improvement in performance required for the next significant step in in vivo MR microscopy.

ACKNOWLEDGMENTS

The authors thank Gary Cofer for assistance with the imaging experiments, Steve Suddarth for help with noise temperature measurements, and Ted Wheeler for animal support.

REFERENCES

1. Black RD, Early TA, Roemer PB, Mueller OM, Mogro-Campero A, Turner LG, Johnson GA. A high-temperature superconducting receiver for nuclear magnetic resonance microscopy. Science 1993; 259:793–795.
2. Black RD, Early TA, Johnson GA. Performance of a high-temperature superconducting resonator for high field imaging. J Magn Reson 1995; 113:74–80.
3. Crowley MG, Evelhoch JL, Ackerman JJH. The surface-coil NMR receiver in the presence of homogenous B_1 excitation. J Magn Reson 1985; 64:20.
4. Bendall MR, Connelly A, McKendry JM. Elimination of coupling between cylindrical transmit coils and surface-receive coils for in vivo NMR. Magn Reson Med 1986; 3:157–163.
5. Picard L, Blackledge M, Decorps M. Improvements in electronic decoupling of the transmitter and receiver coils. J Magn Reson 1995; 106:110–115.
6. Hurlston SE, Brey WW, Suddarth SA, Yap M, Johnson GA. A high-temperature superconducting Helmholtz probe for microscopy at 9.4. T. Magn Reson Med submitted.
7. Jerosch-Herold M, Kirschman RK. Potential benefits of a cryogenically cooled NMR probe for room-temperature samples. J Magn Reson 1989; 85:141–146.
8. Face DW, Wilker C, Kingston JJ, Shen Z-Y, Pellicone FM, Small RJ, McKenna SP, Sun S, Martin PJ. Advances in HTS films for high-power microwave applications. IEEE Trans App Supercon 1997; 7:1283–1286.
9. Gupta KC, Garg R, Chadha R. Computer-Aided Design of Microwave Circuits. Norwood, MA: Artech House; 1981.
10. Withers RS, Liang GC, Cole BF, Johansson M. Thin-film HTS probe coils for magnetic resonance imaging. IEEE Trans App Supercon 1993; 3:2450–2453.
11. Röschmann P, Tischler R. Surface coil proton MR imaging at 2 T. Radiology 1986; 161:251–255.
12. Sorgenfrei BL, Edlestein WA. Optimizing MRI signal-to-noise ratio for quadrature unmatched RF coils: two preamplifiers are better than one. Magn Reson Med 1996; 36:104–110.
13. Miller JR, Zhang K, Ma QY, Mun IK, Jung KJ, Katz J, Face DW, Kountz DJ. Superconducting receiver coils for sodium magnetic resonance imaging. IEEE Trans Biomed Eng 1996; 43:1197–1199.
14. Hübner H, Valenzuela AA. Radiofrequency performance of superconducting thin films in high magnetic fields. Appl Phys Lett 1994; 64:25.
15. Johnson GA, Benveniste H, Black RD, Hedlund LW, Maronpot RR, Smith BR. Histology by magnetic resonance microscopy. Magn Reson Q 1993; 9:1–30.
16. Qiu HH, Cofer GP, Hedlund LW, Johnson GA. Automated feedback control of body temperature for small animal studies with MR microscopy. IEEE Trans Biomed Eng 1997; 44:1107–13.
17. Edelstein WA, Bottomley PA, Pfeifer LM. Signal-to-noise calibration procedure for NMR imaging systems. Med Phys 1984; 11:180–185.
18. Black RD. Noise in high-temperature superconductors. Materials Sci Forum 1993; 287:130–132.
19. Wilker C, Shen Z-Y, Pang P, Face DW, Holstein WL, Matthews AL, Laubacher DB. 5 GHz high-temperature-superconductor resonators with high Q and low power dependence up to 90 K. IEEE Trans Microwave Theory Techniques 1991; 30:1462–1467.
20. Raad A, Kan S. Multi-turn, printed surface coil inductance, and Q optimization. Magn Reson Med 1993; 29:396–397.
21. Ogawa S, Lee TM, Nayak AS, Glynn P. Oxygenation-sensitive contrast in magnetic resonance imaging of rodent brain at high magnetic fields. Magn Reson Med 1990; 14:68–78.
22. Terman FE. Radio Engineers Handbook. New York: McGraw-Hill; 1943.